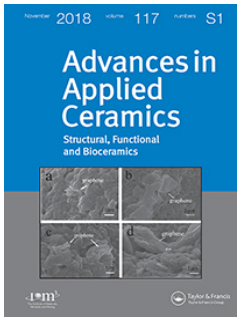

Advances in Applied Ceramics
Structural, Functional and Bioceramics

ISSN: 1743-6753 (Print) 1743-6761 (Online) Journal homepage: https://www.tandfonline.com/loi/yaac20

Influence of zirconium-based alloys on manufacturing and mechanical properties of ultra high temperature ceramic matrix composites

Marius Kütemeyer, Thomas Helmreich, Stefan Rosiwal & Dietmar Koch

To cite this article: Marius Kütemeyer, Thomas Helmreich, Stefan Rosiwal & Dietmar Koch (2018) Influence of zirconium-based alloys on manufacturing and mechanical properties of ultra high temperature ceramic matrix composites, Advances in Applied Ceramics, 117:sup1, s62-s69, DOI: 10.1080/17436753.2018.1509810

To link to this article: https://doi.org/10.1080/17436753.2018.1509810

Published online: 19 Nov 2018.

ADVANCES IN APPLIED CERAMICS
2018, VOL. 117, NO. S1, S62–S69
https://doi.org/10.1080/17436753.2018.1509810

The Institute of Materials, Minerals and Mining
Taylor & Francis
Taylor & Francis Group

Influence of zirconium-based alloys on manufacturing and mechanical properties of ultra high temperature ceramic matrix composites

Marius Kütemeyer[a], Thomas Helmreich[b], Stefan Rosiwal [b] and Dietmar Koch[a]

[a]German Aerospace Center (DLR), Institute of Structures and Design, Stuttgart, Germany; [b]Friedrich-Alexander Universitaet Erlangen-Nürnberg (FAU), Lehrstuhl Werkstoffkunde und Technologie der Metalle, Erlangen, Germany

ABSTRACT

For the continuous development of ultra high temperature ceramic matrix composites manufactured using reactive melt infiltration (RMI), the influence of three different melt alloys and two preform routes on mechanical behaviour and melt infiltration is investigated. Contact angle and viscosity measurement are performed to describe the melt infiltration process. The purpose of these experiments is to further understand the RMI process and increase the mechanical performance of the material. The infiltration height of molten metals within capillary systems depends on the measured contact angles and viscosity as well as the different phases present in the preform, matrix and fibre coating. In order to successfully maintain mechanical performance, minimal reactivity between the melt and coating/fibres is desired. Resulting phase formations, for each manufacturing step, are investigated and analysed using SEM, EDX and XRD. Mechanical performance is determined using flexural strength by three-point-bending, achieving close to 400 MPa with 0/90° fabrics.

ARTICLE HISTORY
Received 28 February 2018
Revised 12 June 2018
Accepted 1 August 2018

KEYWORDS
UHTCMC; ZrB_2; carbon fibre; UHTC; CMC; contact angle; viscosity; RMI

1. Introduction

Ultra high temperature ceramics (UHTCs) are a key factor in hypersonic flight and other extreme temperature applications, reaching 2000°C and higher. Without using active cooling systems, UHTCs are one of the few materials able to withstand these temperatures and to some degree the occurring oxidation, as discussed in several publications [1–5]. In recent years, the focus of UHTC development has concentrated on including fibre reinforcement to increase their damage tolerance. Methods used to manufacture these ultra high temperature ceramic matrix composites (UHTCMCs) are sintering [6], chemical vapour infiltration [4,7] and reactive melt infiltration (RMI) [8,9]. The Focus of this study will be the investigation of melt and preform–matrix interactions occurring during the RMI process, several of which occur at the same time. Phases which do interact are alloy elements (Zr/Cu/Ag/B) and matrix or fibre-coating elements (ZrB_2/TiB_2/B_4C/B/C). The matrix interaction can be separated into interaction prior to and after the chemical reaction. The results are used to neutralise low melting phases by dissolution and formation of more refractory compounds. The advantages and disadvantages of the Zr RMI are comparable to the liquid silicon infiltration (LSI) process, namely low porosity, residual melt and manufacturing of large parts. In case of fibre-reinforced ZrB_2 matrix composite, RMI allows a lower temperature exposure of the fibres compared to HP or SPS, with no additional mechanical pressure. However fibres need to withstand the melt during the RMI process. The purpose of these experiments is to further understand the RMI process and determine the necessary thickness of fibre coatings. The infiltration height of molten metals within capillary systems is highly dependent on their contact angles, and as such, it is important that the chosen element combinations do promote wetting behaviour. In order to successfully maintain mechanical performance, minimal reactions between the melt and coating are desired. This allows for adequate degradation protection without the need for thick coating layers. Melts investigated are Zr_2Cu and Zr_2Ag, including 1 at.-% B additions. Zr_9B is only used for mechanical characterisation, due to its high melting point. A sample using each of these melts is manufactured in combination with a polycarbosilane and phenolic-based preform.

CONTACT Marius Kütemeyer marius.kuetemeyer@dlr.de German Aerospace Center (DLR), Institute of Structures and Design, Pfaffenwaldring 38-40, Stuttgart 70569, Germany

This paper is part of a supplementary issue from the Ultra-High Temperature Ceramics: Materials for Extreme Environment Applications IV conference.

2. Experimental methods

Each process state is analysed and compared via SEM, Zeiss Ultra 55 Plus with Angular selective Backscattered detector (AsB), and EDX from Oxford using a detector size of 20 mm^2. Porosity of pyrolysed preforms is determined by mercury porosimetry, CE Instruments Pascal 240. XRD analysis is performed using a Bruker AXS D8 with Cu Kα (λ = 154 pm). Contact angles are measured using the DSAHT17 system from KRÜSS, up to 1520°C and Ar atmosphere. A peak temperature of 1550°C is set, to be reached via radiative heating. Heating rates are set as follows: 10 K min^{-1} from 25 to 1000°C, 7 K min^{-1} from 1000 to 1200°C and 5 K min^{-1} between 1200 and 1550°C. The influence of differing heating rates is determined during preliminary testing to be minimal, with a variation of less than 10° at any given time across 1000–1500°C (when comparing the chosen heating rate against half-speed). The peak temperature for each experiment, between 1500 and 1550°C, is held for 20 min before cooling begins at a rate of 5 K min^{-1}. The DSA4 camera system takes drop-shape images of the melts shadow and records the associated contact angle; taking 4–5 images K^{-1}. The DSA4 software measures the volume and surface area of the drop as it wets, fitting the silhouette toYoung–Laplace or Tangent algorithms and providing information about the melts spreading behaviour. Viscosity of melts are measured by Anton Paar Germany GmbH using a FRS 1800 DSR 502 system. Different shear rates and temperatures, upon melting to 1400°C or maximum torque, using three different melt alloys are measured. Starting at slightly above melting temperature, the viscosity is measured with a constant shear rate of 15, 25, 50 and 70 s^{-1}, followed by a shear rate ramp from 1 to 75 s^{-1}. Heating ramps are performed under a constant shear rate of 25 s^{-1}. To determine the mechanical behaviour, three-point bending (3PB) tests are performed at room temperatures. The tests are performed according to standard DIN EN 658-3 [10]. The tests are performed with a universal testing machine from Zwick GmbH & Co. KG. Each composition is tested using three samples; the average and standard deviation, considering a normal distribution, is calculated. The ratio of bearing distance and sample thickness is kept at a ratio grater than 20. The upper loading bearing has a radius of 5 mm and the two lower bearing have a radius of 2 mm. The testing speed of each sample was 1 mm min^{-1}.

3. Manufacturing

Similar to LSI, a ZrB_2 formation with Zr-based melts requires attention of the following aspects. A Boron containing porous preform with a capillary system is necessary, which enables liquid melt infiltration. As there are no precursors yet to build boron chains, it is necessary to produce a powder-based slurry which can be infiltrated into fibre bundles. Additionally, the composition of the Zr-based melts needs to be taken into account. Different alloy compositions do influence contact angles, viscosity, phases forming and melting temperature. The three-step process, as described in the previous work [8,9], for UHTCMCs manufactured by RMI is shown in Figure 1. Compared to the previous work, an additional B_2O_3 infiltration of phenolic-based preforms is introduced. This additional step enables the infiltration with Zr alloys without polycarbosilanes.

3.1. Slurry infiltration and pyrolysis

Each precursor is mixed with boron powder, Tradium GmbH amorphous Boron powder 95/97, and impregnated onto fabrics through a foulard (Mathis AG), varying in boron content from 20 to 70 wt-%. Two precursors are used – a polycarbosilane, essentially forming a SiC matrix, and a phenolic, essentially forming C during pyrolysis. Boron is mixed with the precursors prior to handling in a foulard. The foulard has two cylinders rotating under a defined pressure contact. The fibre sheets are stacked into a mould and transferred to a warm press orautoclave for curing. The phenolic-based slurry is infiltrated after drying the stacked fabrics using a vacuum bagging infiltration method.

To prevent the zirconium–carbon reaction during Zr infiltration of the carbon fibres, GRANOC XN-80 weaves are coated with a TiB_2 coating by chemical vapour deposition in a standard CVD reactor (built by Surmetal, Switzerland). The reaction of $TiCl_4$ (flow rate: 0.2 slm) with BCl_3 (flow rate: 0.4 slm) and

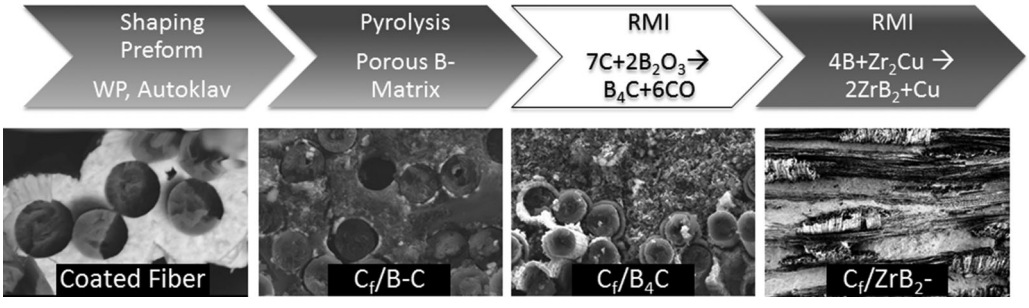

Figure 1. Schematic of the RMI process.

H_2 (flow rate: 10.0 slm) forms TiB_2 and HCl at 800°C. The coating pressure is 300 mbar and the coating time varies between 2 and 4 h, with a growth rate of around 1 μ h^{-1}. During the CVD process, each fabric is placed separate inside the reaction chamber.

Both compositions are pyrolysed at 1300°C in Ar atmosphere. For both precursors, the main mass loss is before reaching 1000°C. From investigating thermogravimetric analysis (TG) and SEM images after pyrolysis, we find that there is no apparent reaction of the boron powder and precursors during pyrolysis cycles.

3.2. Boron oxide infiltration

A method enabling Zr RMI for a phenolic-based boron slurry needs to increase pore diameters and improve the contact angle within the pore structure. Essentially the phenolic resin could be depleted for adaption of the pore size distribution with an additional internal coating of the pore structure after pyrolysis to adapt the contact angle. The coating itself will again influence the pore size distribution due to the deposition of material. Instead the following reaction can be used to influence both factors at once:

$$7C + 2B_2O_3 \longrightarrow B_4C + 6CO \quad (1)$$

Decrease in volume enlarges the pore size distribution and the contact angle will be enhanced due to B_4C formation. B_2O_3 has a melting point of ~475°C and upon melting will start to infiltrate into the capillary system of the preform. The formation of B_4C will start at higher temperatures according to the literature [11–13]. Jung et al. [12] describes the influence of pyrolysis temperature, dwelling time and carbon content on the formation of B_4C. Figure 2 shows a SEM image of a phenolic-based pyrolysed composite on the left and the same composition after B_2O_3 infiltration and pyrolysis at 1800°C on the right. Most of the amorphous carbon is being transformed into B_4C, leaving a larger pore structure.

Figure 3 shows the pore size distribution of the different precursors, polycarbosilane, phenolic resin and phenolic resin after B_2O_3 infiltration. Polycarbosilane has a very large bandwidth of larger pores compared to phenolic resin. Pore size distribution of B_2O_3 infiltrated sample are similar in bandwidth and size to polycarbosilane samples and therefore promote infiltration with Zr alloys. Once the carbon is consumed, additional infiltration cycles do not change the pore size distribution further, as shown by the bottom graph of Figure 3. This is also observed by measuring overall porosity and mass change during pyrolysis. The amount of B_2O_3 can be calculated by the ceramic yield of the phenolic resin and the fibre volume content. Besides contact angles and overall porosity, adopted pore sizes are essential for Zr-based RMI. The formation of ZrB_2 and ZrC do include a volume expansion, when compared with the volume of C or B. If the pore sizes are too small, they are blocked by the volume expansion and infiltration is chocked. Figure 4 shows an XRD analysis of a pyrolysed phenolic slurry-based sample, including carbon fibres, in comparison to an identical sample infiltrated with B_2O_3. Each sample is pyrolysed at 1300°C and infiltration is taken to 1800°C in order to start B_4C formation, both in Ar atmosphere. The XRD shows that both B and B_4C signals become more prominent. This is due to the formation of B_4C and consumption of the amorphous C, from the phenolic precursor. As described in the SEM images in Figure 2. TG analysis of pure B_2O_3 powder and carbon from a pyrolysed phenolic with B_2O_3 powder up to 1600°C shows a mass loss of the mixture being slightly lower due to the formation of B_4C instead of evaporation of the B_2O_3. At 1400°C evaporation of the B_2O_3 becomes much more rapid, as seen by rapid increase of mass loss of pure B_2O_3. In order to promote B_4C formation heating rates from 1400°C onward should be at max.

3.3. Reactive melt infiltration

Melt infiltration is performed as described by Kütemeyer et al. [8,9], heating melt and samples separate

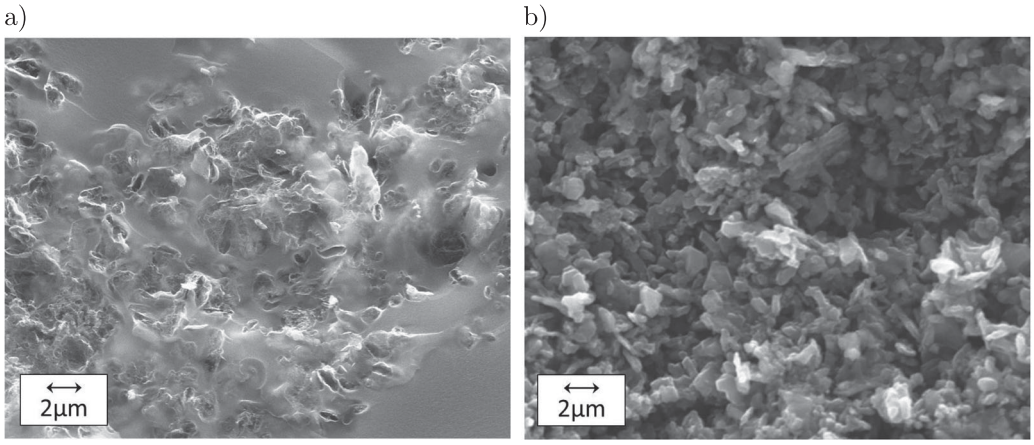

Figure 2. Matrix micro-structure before (a) and after B_2O_3 infiltration (b).

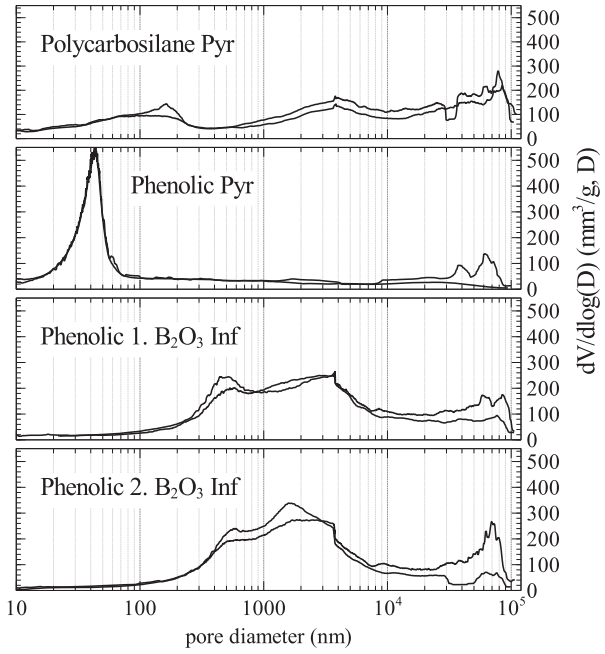

Figure 3. Pore size distribution of pyrolysed polycarbosilane, phenolic resin and phenolic resin after B_2O_3 infiltration.

from each other in order to control infiltration temperature, ranging from 1500 to 1900°C. As shown in the previous work, TiB_2 is a suitable protection for carbon fibres during the RMI process. Oxidation resistance of TiB_2 at ultra high temperatures is, however, inferior compared to ZrB_2 [3,14,15]. Hence the TiB_2 coating thickness should be as thin as possible. In addition, a thick fibre coating will start to seal the fibre bundles, not allowing any boron slurry or melt to infiltrate into the fibre bundles. Figure 5 shows the TiB_2 coating thickness after (a) 2 h and (b) 4 h of CVD process time. Due to the linear behaviour of this process, as long as bundles are not sealed and surface areas start to change rapidly, the 4 h process produces twice the coating thickness of around 4 μm.

In addition to contact angles, viscosity of the melts influences infiltration. Figure 6 shows the viscosity of Zr_2Cu, Zr_2Cu-1 at.-%B and Zr_2Ag-1 at.-%B over

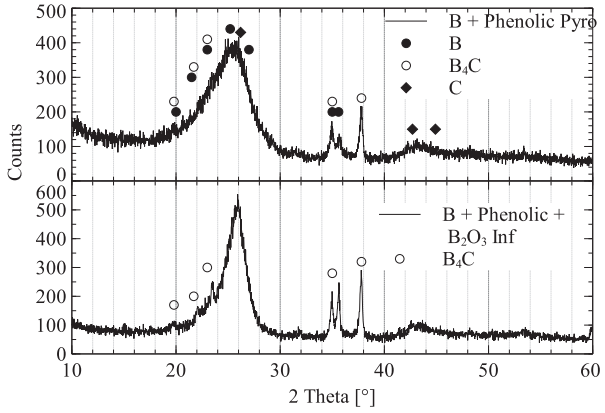

Figure 4. XRD of pyrolysed phenolic samples with and without B_2O_3 infiltration.

temperature at shear rates of 10, 25 and 50 s^{-1}. Zr_2Cu, being the only one with no B addition, shows an expected decrease in viscosity when temperature is raised. Both alloys containing B do increase rapidly in viscosity within 100°K upon melting. All of them do decrease in viscosity with increasing shear rates. Upon melting Zr_2Cu and Zr_2Cu-1 at.-%B are similar in viscosity. In the range of 1000–1100°C, Zr_2Cu-1 at.-%B starts increasing in viscosity, while Zr_2Cu does become lower in viscosity. Zr_2Ag-1 at.-%B decreases in viscosity until 1350°C, showing an increases in viscosity at 1400°C. Experiments have been performed with graphite crucibles, which can cause reactions with the liquid Zr or changing the alloy composition to include C. SEM and EDX analysis show a small ZrC layer on the crucible and rod after testing. Micro-structures of Zr_2Cu-1 at.-%B and Zr_2Ag-1 at.-% B show scersed ZrB_2 particles as well as Zr rich phases inside the Zr_2Cu/Zr_2Ag melt after the tests. Both melts also infiltrate a few mm into the carbon crucible and rod. Measurements from Zr_2Cu are more stable when increasing shear rates as compared to Zr_2 Cu-1 at.-% B, may be due to the formation of ZrB_2 particles within the melt. Slightly above melting temperature, 1027°C, both alloys do have similar viscosity across the shear rate spectrum. Until 1350°C Zr_2Ag-1 at.-%B has the lowest viscosity of the tested melts.

Due to comparison, each of the tested samples is infiltrated at 1500°C using Zr_2Cu-1 at.-%B and Zr_2Ag-1 at.-%B alloys, additional infiltrations at 1900°C for a Zr_9B alloy are performed. Lower infiltration temperatures are not possible for the polycarbosilane samples due to a large volume expansion described by Kütemeyer et al. [9]. Each sample is heated separate from the melt and upon reaching 1500°C is lowered into the melt. To further increase capillary force, infiltration are performed in vacuum atmosphere. Figure 7 shows the contact angles of Zr_2Cu, Zr_2Ag, Zr_2Cu-1 at.-%B and Zr_2Ag-1 at.-%B melts on C and SiC substrate to determine their performance for RMI. SiC is an important substrate to determine the wetting behaviour of each melt for polycarbosilane sample infiltration. The Ag-based alloys immediately drop in contact angle on SiC after melting, Cu-based alloys keep constant for around 300°K on SiC before dropping to low contact angles ($< 5°$). For both substrates and alloy types, B addition lower the contact angles. Zr_2Cu and Zr_2Cu-1 at.-%B do not drop under 25° on C substrates, which is why infiltration of samples with high C content only infiltrates a few mm. Contact angles for B_4C substrates will be determined while continuing RMI research.

From contact angle measurements two different melts are determined to be using as infiltration alloys. Zr_9B is chosen as an additional candidate for these investigations, even though its contact angle could not be determined due to its high melting point. The

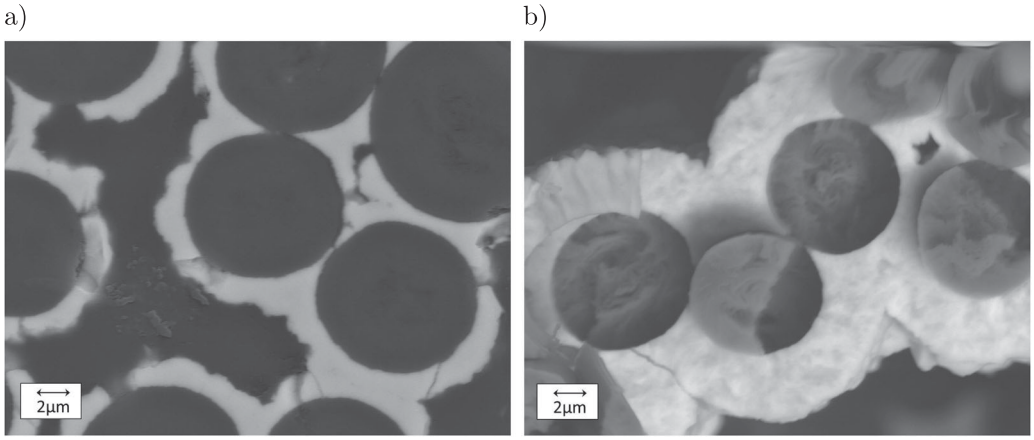

Figure 5. Carbon fibres with TiB_2 coating after (a) 2h and (b) 4h CVD coating time.

advantage of Zr_9B is the absence of any low melting phases and large ZrB_2 grain, which form during RMI. All trials are performed with the same heating rates, dwelling time at peak temperature and infiltration times. The infiltration time is set to 20 min, ensuring a full infiltration of each sample. Each preform manufacturing rout is tested with each of the alloys and evaluated according to its mechanical properties and phases formed within its micro-structure, shown in Figure 8. In each of the six variations, ZrB_2 and ZrC are the main phases. The different alloys do influence the residual melt in between the UHTC grains. Both preform manufacturing methods show similar fracture surface on 3PB tests. The main difference in fracture surfaces is between the different melts used for infiltration. While Zr_2Cu-1 at.-%B and Zr_2Ag-1 at.-%B are similar, the Zr_9B infiltrated samples have a different fracture behaviour, as shown exemplary for the phenolic preform in Figure 9. The different behaviour is due to the incomplete infiltration of the fibre bundles, when using the Zr_9B alloy. Either the viscosity of the alloy is not low enough to fully infiltrate the bundles, or the formation of ZrC and ZrB_2 and their volume expansion is preventing a full infiltration.

Table 1 shows the result of 3PB tests performed for each melt and preform. Zr_2Cu-1 at.-%B reaches the highest bending strength and ultimate strain, with the polycarbosilane-based preform being slightly higher than the phenolic based. All specimens initialised a crack on the bottom side under tensile loading. Every combination does show fibre pull-out and crack deflection. However, these mechanisms are not as distinct as in previous works [9], most likely due to the thinner TiB_2 fibre coating.

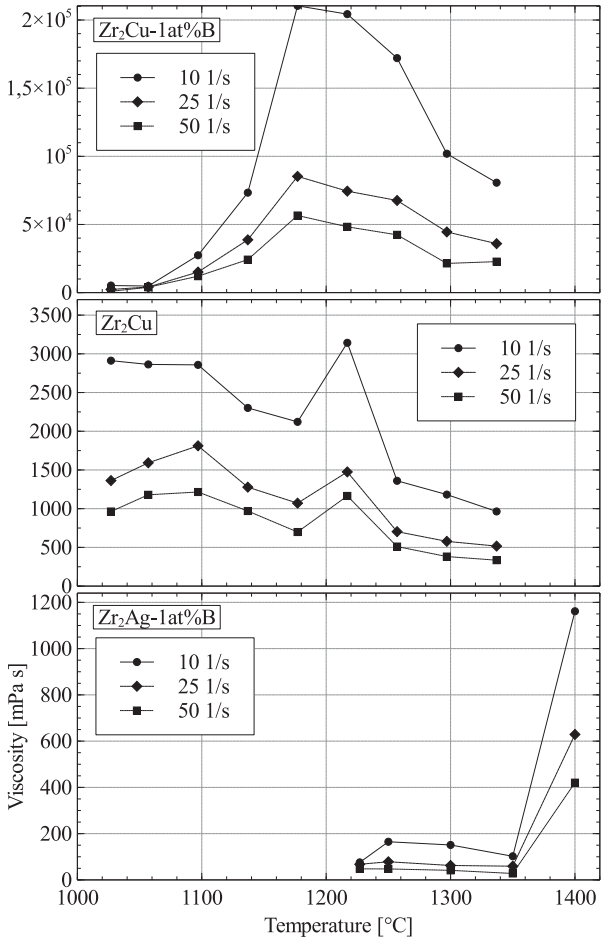

Figure 6. Viscosity in dependence of temperature at three different shear rates for different melts.

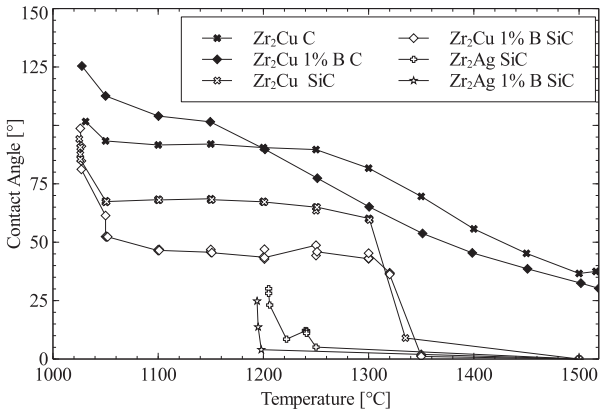

Figure 7. Contact angles of different melt alloys on C and SiC substrates.

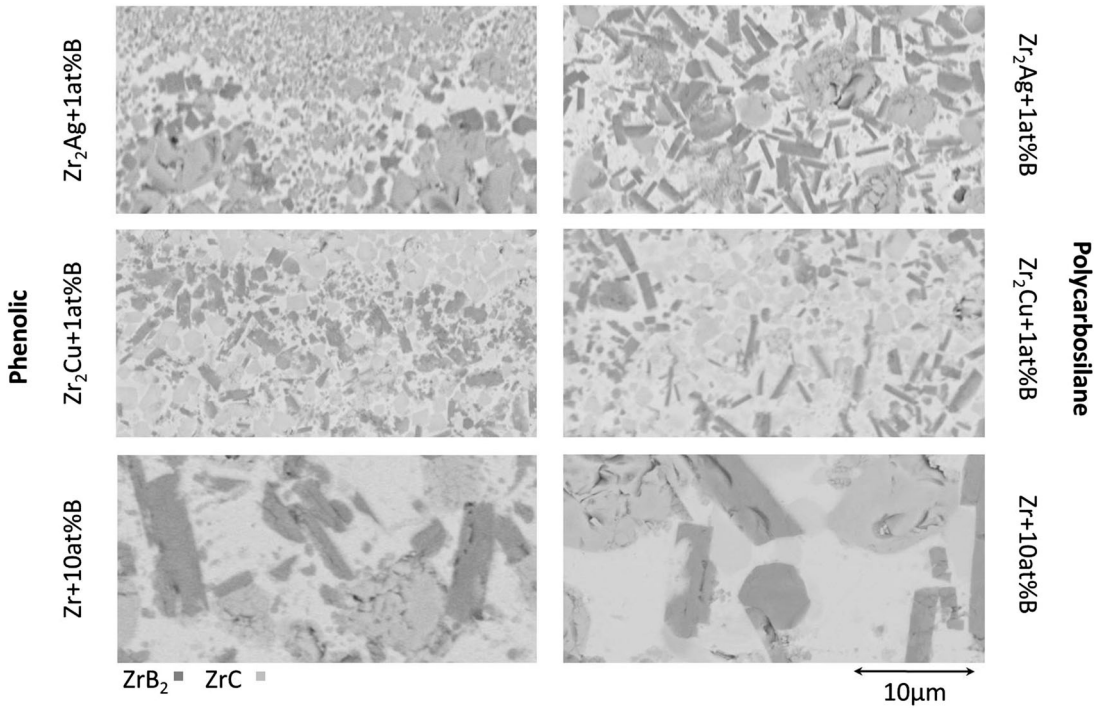

Figure 8. Matrix variations within the micro-structure when using different melts and preforms.

4. Discussion

Infiltration of B_2O_3 does essentially decrease ceramic yield of preforms by mass loss due to CO formation. In terms of RMI for ZrB_2 a high porosity and low C contents are favourable. Most critical for the B_2O_3 treatment is an eventual fibre degradation. As the Zr melt, the B_2O_3 does infiltrate using the capillary system of the preform, also reaching within the fibre bundles. Due to the TiB_2 fibre coating, already protecting the fibres from Zr melt, this aspect is not causing any problems upon manufacturing. Evaporation of the B_2O_3, as shown by TG measurements, does need to be compensated by additional B_2O_3 and fast heating rates above 1400°C. Additional investigations will show, whether B_2O_3 does infiltrate as a liquid into the pore system or as a gas phases upon evaporation. Compared to UHTCMC infiltrated by Kütemeyer et al. [9], carbon fibres in this work have been coated with 2 μm TiB_2 instead of 4 μm. Therefore, more fibres are degraded during RMI, forming a matrix dominant behaviour. Highest bending strength is

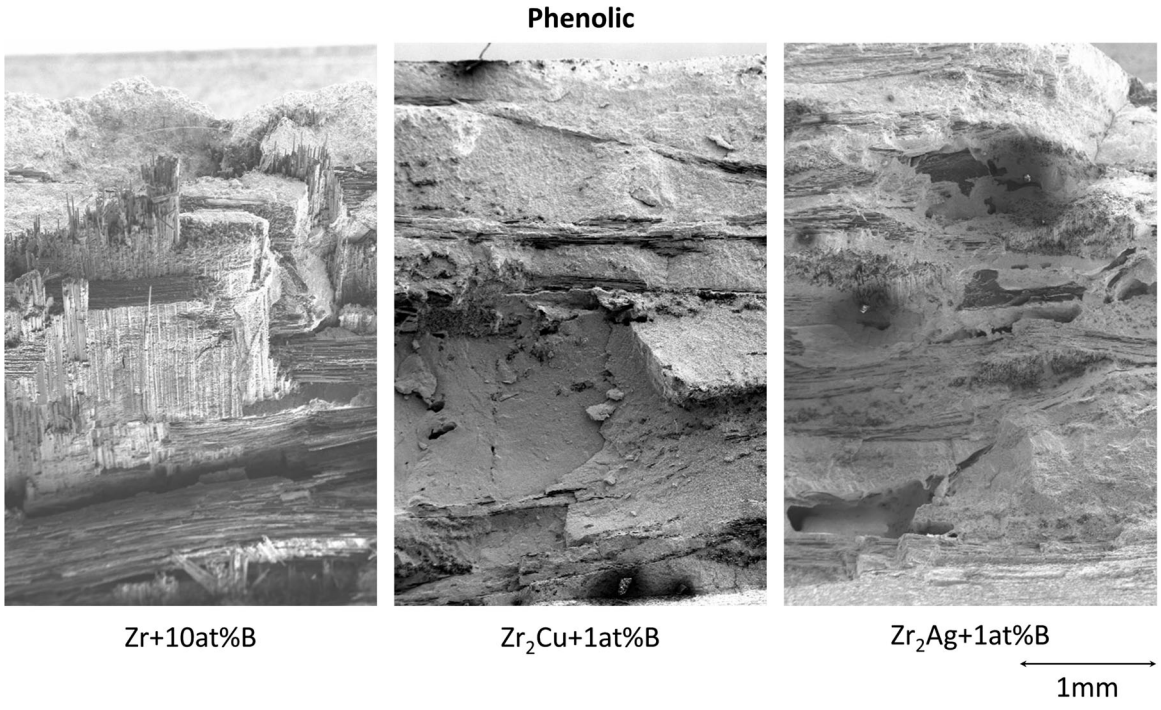

Figure 9. Fracture surface after 3PB of the phenolic preform for each of the three melts.

Table 1. Mechanical properties, ultimate stress σ_U, modulus E and ultimate strain e_U, of tested melt and preform combinations.

	σ_U [MPa]		E [GPa]		e_U [%]	
	PCS	PH	PCS	PH	PCS	PH
Zr_2Cu-1 at.-%B	393 ± 27	363 ± 10	147 ± 2	183 ± 10	0.39 ± 0.09	0.21 ± 0.01
Zr_2Ag-1 at.-%B	134 ± 21	78 ± 19	210 ± 86	128 ± 10	0.07 ± 0.02	0.15 ± 0.09
Zr_9B	190 ± 32	181 ± 81	144 ± 13	162 ± 25	0.16 ± 0.06	0.14 ± 0.09

Note: polycarbosilane (PCS) and phenolic (PH).

achieved using the Zr_2Cu-1 at.-%B melt with very little difference between polycarbosilane and phenolic preform, see Table 1. Beside the absence of Cu phases within the Zr_9B infiltrated samples, the ZrB_2 grain forming within these samples are much large by almost a factory of 10. Both larger grains and higher infiltration temperature could influence bending strength. Zr_2Ag-1 at.-%B infiltrated samples generate the lowest bending strength. By examining the tested samples, larger crack like pores are found within the matrix of the samples. They appear to be more frequently between each fabric layer. These pores could either be forming due to the lower viscosity of the Ag-based melts, draining the centre of large pore channels. They could also be forming by evaporating Ag having a boiling point of 2210°C, which could be reached by the exothermic reaction, further increasing samples temperature from 1500°C at initialising infiltration. Cu would increase this temperature limit to a boiling point of around 2595°C.

Beside viscosity and different phases forming, the governing influence for RMI are the contact angles forming. While Zr alloys drop in contact angle to about 25° on C substrates, they are not infiltrating preforms containing high C contents. Further research should investigate, whether contact angles of 25° on C are only reached do to the formation of ZrC. SiC substrates, representing polycarbosilane behaviour, do drop in contact angle at around 1300°C and start to show sufficient infiltration, see Figure 7, which could also occur do to ZrC formation.

5. Conclusion

As described, a phenolic-based preform in combination with a B_2O_3 infiltration enables a Zr alloy-based RMI. Bending strength are almost the same as polycarbosilane-based sample, but manufacturing costs are lower. Zr_2Cu-1 at.-%B melts reach 393 MPa 3PB strength compared to 190 MPa of Zr_9B at room temperature. Cu phases are low within the Zr_2Cu-1 at.-%B samples and can be reduce further, however high temperature strength might be less influenced when using the Zr_9B melt. Without having the limitation from volume expansion by the phases forming at temperatures below 1500°C, when using a polycarbosilane-based preform, infiltration temperatures can be further reduced without interrupting RMI. Further investigations will concentrate on the opportunity to manufacture UHTCMC at temperature below 1500°C.

Acknowledgement

This paper was originally presented at the Ultra-High Temperature Ceramics: Materials for Extreme Environments Applications IV Conference (Windsor, UK) and has subsequently been revised and extended before consideration by *Advances in Applied Ceramics*.

Disclosure statement

No potential conflict of interest was reported by the authors.

Funding

This work has received funding from the European Unions Horizon 2020 Research and Innovation Programme under grant agreement Nr. 685594 (C3HARME).

ORCID

Stefan Rosiwal http://orcid.org/0000-0002-5728-0635

References

[1] Glass DE. Physical challenges and limitations confronting the use of UHTCs on hypersonic vehicles. AIAA. 2011.
[2] Loehman R, Corral EL, Dumm HP, et al. Ultra high temperature ceramics for hypersonic vehicle applications. 2006. (Sandia Report).
[3] Opeka MM, Talmy IG, Zaykoski JA, et al. Oxidation-based materials selection for 2000°C + hypersonic aerosurfaces. Theoretical considerations and historical experience. J Mater Sci. 2004;9:5887–5904.
[4] Paul A, Jayaseelan DD, Lee W. UHTC composites for hypersonic applications. ACS Appl Mater Interface. 2011. 2011.
[5] Scatteia L, Borrelli R, Marino G, et al. Characterization and process of new metal diboride compound for TPS applications. AIAA/CIRA 13th International Space Planes and Hypersonic Systems and Technology Proceedings American Institute of Aeronautics and Astronautics, Reston, VA. 2005.
[6] Zoli L, Sciti D. Efficacy of a ZrB_2-SiC matrix in protecting C fibres from oxidation in novel UHTCMC materials. Mater Design. 2017;113:207–213.
[7] Paul A, Rubio V, Binner J, et al. Evaluation of the high temperature performance of hfb2 uhtc particulate filled cf/c composites. Int J Appl Ceram Technol. 2017;14 (3):344–353.
[8] Kütemeyer M, Shandler D, Koch D, et al. Reactive melt-infiltration of boron containing fiber reinforced preforms forming a ZrB2 matrix. In: Mahmoud MM, Bhalla AS, Bansal NP, et al., editors. *Ceramic Transactions*. Hoboken (NJ): John Wiley & Sons; 2015. p. 464.

[9] Kütemeyer M, Schomer L, Helmreich T, et al. Fabrication of ultra high temperature ceramic matrix composites using a reactive melt infiltration process. J Eur Ceram Soc. 2016 Nov;36(15):3647–3655. Available from: http://www.sciencedirect.com/science/article/pii/S0955221916302151.
[10] Deutsches Institut für Normung. DIN EN 658-3: Hochleistungskeramik - Mechanische Eigenschaften von keramischen Verbundwerkstoffe bei Raumtemperatur - Teil 3: Bestimmung der Biegefestigkeit; 2002.
[11] Alizadeh A, Taheri-Nassaj E, Ehsani N. Synthesis of boron carbide powder by a carbothermic reduction method. J Eur Ceram Soc. 2004;24 (10):3227–3234.
[12] Jung CH, Lee MJ, Kim CJ. Preparation of carbon-free B_4C powder from B_2O_3 oxide by carbothermal reduction process. Mater Lett. 2004;58(5):609–614.
[13] Singh P, Singh B, Kumar M, et al. One step reduction of Boric Acid to boron carbide nanoparticles. Ceram Int. 2014;40(9 PART B):15331–15334.
[14] Parthasarathy TA, Rapp RA, Opeka M, et al. A model for the oxidation of ZrB_2, HfB_2 and TiB_2. Acta Mater. 2007;55(17):5999–6010. Available from: http://www.sciencedirect.com/science/article/pii/S1359645407004752.
[15] Kaufman L, Clougherty EV. Investigation of boride compounds for very high temperature applications. Wright-Patterson Air Force Base, Ohio: ManLabs Inc.; 1965.